

Towards Discovery of Polymers for Insulin Delivery via Physics-Grounded Agentic Workflows

Martins Otun¹

¹Algonix AI Ltd., Scotland, United Kingdom

Cold-chain storage limits access to insulin for hundreds of millions of people; a thermally protective patch polymer could help, but the design space is too large for exhaustive experiment. Starting from that problem, we narrow to an agentic workflow: a large language model (LLM) calls physics-based tools through the Model Context Protocol (MCP), searching the discrete PSMILES space under a budget of OpenMM Packmol-matrix evaluations. The LLM acts as an implicit acquisition function conditioned on a persistent “discovery world”: hypotheses, literature claims, and simulation outcomes updated each iteration. Under matched oracle budgets, the best autonomous campaign reaches an insulin–polymer interaction energy of -2263 kJ/mol, outperforming reinforcement-learning baselines by 68% and Bayesian optimization by 19%. Three independent campaigns converge on one structural motif (dense hydrogen-bond donors and acceptors per repeat unit) while physics checks reject infeasible packings and name–structure mismatches before they steer the next step. The science stage is CPU-bound and runs on commodity hardware. More broadly, the same architecture and workflow designed here applies to other protein-stabilization tasks whenever a tractable screening oracle is available.

Code: <https://github.com/otunmartins/FRIDGEFREENET>

Correspondence: O.M. (martins@algonix.co.uk)

1 Introduction

Diabetes affects over 500 million people worldwide, and its management depends critically on insulin that must be stored between 2 and 8°C [7]. In resource-limited settings, where refrigeration is unreliable or absent, this cold-chain requirement leads to degraded medication and preventable complications. A transdermal patch whose polymer matrix stabilizes insulin at ambient temperature would fundamentally change access to treatment, but the combinatorial space of candidate polymers is vast, and no single experimental campaign can screen more than a tiny fraction of it.

Polymer informatics has begun to narrow this space computationally. Machine-readable repeat-unit notations such as PSMILES [11, 13] and graph-neural-network property predictors trained on curated databases [5, 8, 10] enable rapid surrogate evaluation. However, surrogate models approximate physical reality rather than simulate it; they cannot catch sterically infeasible packings or reject chemically implausible structures that happen to score well on a learned surface. What is missing is a closed loop in which candidate generation, explicit molecular simulation, and hypothesis revision operate together so that each iteration is grounded in physics rather than interpolation.

Meanwhile, large language model (LLM) agents have

demonstrated the ability to orchestrate multi-step scientific workflows. Boiko et al. showed autonomous chemical synthesis planning [3], Zheng et al. applied ChatGPT to metal–organic framework prediction [32], and the Kosmos system combined parallel agents through a shared world model for multi-domain discovery [19]. Stephens and Salawu formalized such agentic processes as probability chains over tool calls, providing a mathematical vocabulary for analyzing how state updates, inference functionals, and action-space partitioning affect the likelihood of reaching a goal [28]. Those examples emphasize synthesis planning, porous-crystal prediction, or cross-domain literature agents rather than budgeted search over polymer repeat units with explicit energy evaluation against a specified protein structure between hypothesis updates. Complementary work increasingly connects LLMs to molecular dynamics and simulation stacks, including simulation-informed training of MD assistants [26], natural-language control of MD engines [9], and autonomous simulation agents for polymer benchmark workflows [14].

In this work, we focus on a different closed loop that combines literature mining, cheminformatics, and molecular simulations to screen a range of polymeric materials. We instantiate this design as an agentic discovery platform built on the Model Context Protocol (MCP) [2]. The platform exposes literature mining, PSMILES validation,

cheminformatics mutation, and OpenMM Packmol-matrix screening as callable tools; a persistent “discovery world” accumulates hypotheses, simulation outcomes, and literature claims across iterations. Formally, we cast the search as budget-constrained optimization over the discrete PSMILES space, where the LLM serves as an implicit acquisition function [31] conditioned on a structured state that classical optimizers lack [25]. The simulation stage is CPU-bound, so the entire workflow runs on commodity hardware, compatible with the local and edge LLM deployments gaining traction in resource-constrained laboratories [30].

The paper is organized as follows. First, we formalize the agentic discovery loop using the probabilistic-chain framework of Stephens and Salawu and budget-constrained regret theory, and we compare the degrees of freedom available to RL, Bayesian optimization, and LLM-agent strategies (§2). Second, we benchmark DQN, PPO, and Optuna TPE against three independent 25-iteration autonomous LLM campaigns on the same physics objective, showing that the agentic workflow reduces simple regret by up to 68% over RL (§3). Third, we analyze the chemical reasoning recorded in the discovery world, demonstrating cross-campaign convergence on hydrogen-bond-dense motifs and quantifying how physics-based falsification prunes hallucinated or sterically untenable proposals (§4).

2 Methods

2.1 Platform architecture

We implement the platform as a single Python MCP server [2] (FastMCP) that registers tools for literature mining, polymer validation, molecular screening, cheminformatics mutation, and session management. It runs inside the `insulin-ai-sim` conda environment, which bundles OpenMM [4], RDKit [12], Packmol [18], the Open Force Field toolkit [22], and Stable-Baselines3 [24]. An LLM hosted by OpenCode (or Cursor) connects to this server and calls tools in response to user prompts; model weights, tool schema, and session artifacts are version-controlled alongside the scientific code.

Figure 1 summarizes the data flow. Each discovery session creates a folder under `runs/<session_id>/` containing per-iteration state files (`agent_iteration_N.json`), a structured world-model rollout (`discovery_world.json`), cumulative best-candidate records (`ALL_ITERATIONS_BEST_CANDIDATES.tsv`), structure artifacts (PDB, PNG), and a compiled summary report (Markdown and PDF).

2.2 Problem formulation

We formalize the agentic loop at two complementary levels: a *probabilistic chain* that describes the agent’s action sequence [28], and a *budget-constrained optimization* that defines the search objective [25].

Table 1 Degrees of freedom available to each search method, following the probabilistic-chain framework of Stephens and Salawu [28].

	\mathcal{F}	u	$s_0(c)$	$\{\alpha\}$
RL	policy net	\emptyset	PEG seed	mutations
TPE	sampler	\emptyset	seed	mutations
LLM	π_{LLM}	u_{sel}	prompt+world	MCP tools

Probabilistic chain (agent level). Following Stephens and Salawu [28], we model the discovery loop as a chain of conditional probabilities over tool calls. Given an initial context c (user objective, tool schema, and seed state), the probability of executing an action sequence $\mathbf{a} = (a_1, \dots, a_n)$ is

$$P(\mathbf{a} | c) = \prod_{i=1}^n P(a_i | s_{i-1}, c), \quad (1)$$

where $s_0 = s_0(c)$ is the initial prompt state and $s_i = u(a_i, s_{i-1})$ is the state update [21]. Under the ReAct formalism the LLM generates a reasoning trace (“thought”) t_i before each tool call, so

$$P^t(a_i | s_{i-1}) = P(a_i | t_i, s_{i-1}) P(t_i | s_{i-1}). \quad (2)$$

Each action decomposes as $a_i \rightarrow (\alpha_i, x_i, o_i)$, where $\alpha_i \in \{\text{mine, generate, mutate, screen, patch_world}\}$ is the MCP tool class, x_i is its argument, and o_i is the returned observation.

Different search strategies occupy different positions in this framework depending on the optimization levers (the *degrees of freedom*) available to each (Table 1). RL agents use a fixed policy network \mathcal{F} , no persistent state update ($\mathcal{W}_t = \emptyset$), and a small mutation library $\{\alpha\}$. Optuna adds an explicit acquisition function (tree-structured Parzen estimator) but still lacks hypothesis-level reasoning. The LLM agent has access to all levers: an inference functional \mathcal{F} that improves through in-context learning, a structured selective state update $u_{\text{selective}}$ (the discovery world), and the full MCP tool set. Per Stephens and Salawu [28], MCP provides standardized tool schemas and argument syntax that constrain the action space, improving $P^{\mathcal{F},u}(a_i | s_{i-1})$ relative to unconstrained generation.

Budget-constrained optimization (search level). Let \mathcal{X} denote the discrete space of valid PSMILES and let $f : \mathcal{X} \rightarrow \mathbb{R}$ be the noisy screening oracle that returns the interaction energy,

$$f(x) = E_{\text{int}}(x) + \epsilon, \quad \epsilon \sim \mathcal{N}(0, \sigma^2), \quad (3)$$

where σ captures stochastic packing variability ($\sim 15\%$ in our protocol). The agent selects candidates x_1, \dots, x_B

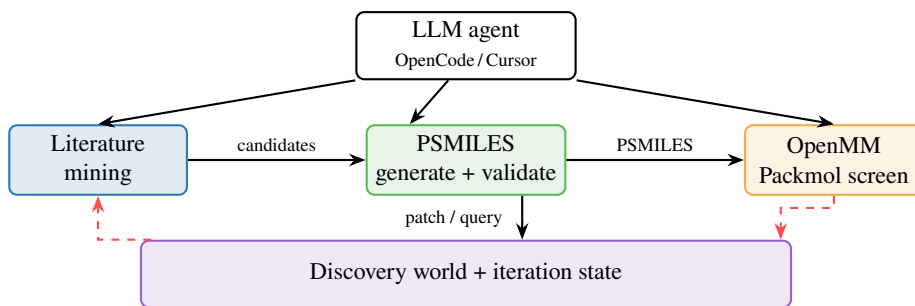


Figure 1 Platform architecture. Solid arrows denote tool calls from the LLM agent; dashed arrows show feedback paths through the session state. The discovery world file persists hypotheses, literature claims, and simulation outcomes for cross-iteration planning.

under oracle budget B ; the goal is to minimize the *simple regret* [25, 27]

$$r_B = f(x^*) - \min_{t \leq B} f(x_t). \quad (4)$$

Classical Bayesian optimization chooses the next query by maximizing an explicit acquisition function $\alpha(x | \mathcal{D}_t)$ such as expected improvement or GP-UCB [27]. The LLM agent instead implements an *implicit acquisition* [15, 31],

$$x_{t+1} = \pi_{\text{LLM}}(s_t) \approx \arg \max_{x \in \mathcal{X}} \alpha_{\text{implicit}}(x | \mathcal{D}_t, \mathcal{W}_t), \quad (5)$$

conditioned on the full state $s_t = (\mathcal{D}_t, \mathcal{W}_t, \mathcal{H}_t)$, which includes the evaluation history \mathcal{D}_t , the discovery-world hypotheses \mathcal{W}_t , and the LLM’s implicit belief \mathcal{H}_t . Iterations that *falsify* a hypothesis (packing failures, name–structure mismatches) contribute high information gain

$$I_t = H(\mathcal{H}_t) - H(\mathcal{H}_t | o_t, \mathcal{W}_{t+1}) \quad (6)$$

even when $f(x_t)$ is poor. Such observations are wasted budget under RL or Optuna (which have no hypothesis state \mathcal{W}_t) but valuable in the agentic loop because they prune unpromising chemical families from future exploration.

2.3 Discovery world model

Inspired by the structured world model in Kosmos [19], we maintain a session-scoped JSON document (`discovery_world.json`) that accumulates:

- **Objective and history:** the user’s research goal and any mid-campaign steering notes.
- **Literature entries:** stable IDs, titles, one-sentence claims, source iteration, and optional DOI or Semantic Scholar identifiers.
- **Simulation entries:** PSMILES, interaction energy, screening status, and pointers to structure artifacts.
- **Hypotheses:** free-text statements with supporting evidence IDs and a status tag (open, supported, weak, dropped).
- **Open questions and human directives:** recorded per iteration for traceability.

Three MCP tools operate on this file: `patch_discovery_world` merges id-keyed lists (update existing or append new entries); `discovery_world_planning_context` returns a bounded text digest for prompt construction; and `get_discovery_world_state` provides full or summarized JSON for inspection. When the agent calls `save_discovery_state` after each iteration, the server automatically updates `meta.last_iteration` and links the latest `agent_iteration_N.json` into the world file, ensuring the rollup stays synchronized without requiring the model to issue a second patch.

2.4 Agentic discovery loop

A single iteration proceeds as follows:

1. **Literature mining.** The agent queries Semantic Scholar [16] (or an Asta-backed corpus when an API key is available) with an adaptive query derived from the world model’s hypotheses, open questions, and prior top performers.
2. **Candidate generation.** Material names from the literature are converted to PSMILES via a curated 60-polymer lookup table with PubChem fallback (automated polymerization-site detection for vinyl, ester, and amide monomers). Each candidate is validated with RDKit (connectivity, valence, exactly two [*] connection points) and cross-checked against PubChem monomer Tanimoto similarity.
3. **OpenMM screening.** Validated PSMILES are evaluated by the Packmol-matrix protocol: short polymer oligomers are packed around insulin (PDB 4F1C), the composite is energy-minimized with the GAFF/OpenFF force field for polymers and AMBER ff14SB for the protein [6, 17, 22], and the insulin–polymer interaction energy is computed.
4. **Mutation.** A cheminformatics mutator generates derivative PSMILES from top performers via functional-group substitution, backbone extension, and random fragment recombination, optionally guided by feedback on problematic substructures.

Algorithm 1 Agentic Discovery Loop

Require: context c , oracle f , budget B

```
1:  $s_0 \leftarrow s_0(c)$  ▷ prompt + tool schema
2:  $\mathcal{W}_0 \leftarrow \emptyset$ ;  $\mathcal{D}_0 \leftarrow \emptyset$ 
3: for  $t = 1, \dots, B$  do
4:    $t_i \leftarrow$  LLM reason over  $s_{t-1}$  ▷ Eq. 2: thought
5:    $\alpha_i \leftarrow$  select MCP tool class from {mine, gen, mut, scr}
6:    $x_i \leftarrow$  LLM generate tool argument
7:    $o_i \leftarrow \alpha_i(x_i)$  ▷ execute tool call
8:   if  $\alpha_i = \text{screen}$  then
9:      $y_i \leftarrow f(x_i)$  ▷ Eq. 3: noisy oracle
10:     $\mathcal{D}_t \leftarrow \mathcal{D}_{t-1} \cup \{(x_i, y_i)\}$ 
11:   end if
12:    $s_t \leftarrow u_{\text{sel}}(a_i, s_{t-1})$  ▷ Eq. 1: state update
13:    $\mathcal{W}_t \leftarrow \text{patch\_world}(\mathcal{W}_{t-1}, o_i, t_i)$ 
14: end for
15: return  $\arg \min_{x \in \mathcal{D}_B} f(x)$ 
```

- 5. State persistence.** The agent saves iteration state, patches the world model with new literature and simulation entries, updates hypotheses, and appends the best candidate to a cumulative TSV.

In *human-in-the-loop* mode the agent pauses after step 5 for user feedback; in *autonomous* mode it immediately proceeds to the next iteration, stopping after N cycles or upon energy-threshold or saturation criteria.

Algorithm 1 formalizes this loop using the notation from §2.2.

2.5 Molecular screening protocol

The screening objective is the non-bonded interaction energy between insulin and a polymer shell. For each candidate PSMILES, the server: (a) generates a 3D oligomer conformer with RDKit; (b) packs n polymer chains around insulin using Packmol [18] at a target density; (c) assigns GAFF2/OpenFF parameters to the polymer and AMBER ff14SB to insulin; (d) runs a two-stage energy minimization (steepest descent followed by L-BFGS); (e) optionally performs a short NPT equilibration at 310 K and 1 bar using the LangevinMiddleIntegrator [4] with a 2 fs timestep. The interaction energy E_{int} is defined as

$$E_{\text{int}} = E_{\text{complex}} - E_{\text{insulin}} - E_{\text{polymer}} \quad (7)$$

where each term is the potential energy of the specified subsystem after minimization. More negative values indicate stronger insulin–polymer attraction. Each call to `evaluate_candidates` corresponds to one oracle query $f(x_t)$ (Eq. 3), returning observation $o_t = (x_t, y_t, \text{status}_t)$. This single-point heuristic does not replace free-energy calculations but provides a computationally tractable ranking across hundreds of candidates.

Candidates that fail RDKit parsing, violate prescreen chemistry rules (e.g. forbidden elements, excessive molecular weight), or exceed Packmol packing timeouts are logged

with verbatim failure reasons and excluded from energy rankings.

2.6 Benchmark methods

To contextualize the agentic workflow, we benchmark three non-agentic search strategies under a matched evaluation budget of $B=160$ successful OpenMM screenings.

DQN and PPO reinforcement learning. We adapt an RL formulation [3] to polymer discovery. In the notation of §2.2, both agents operate on a degenerate state $s_t = (x_t^{\text{best}}, y_t^{\text{best}})$ with no world model ($\mathcal{W}_t = \emptyset$), a fixed policy network as inference functional \mathcal{F} , and the mutation library as their only action set $\{\alpha\}$ (Table 1). Actions select from functional-group swap, backbone extension, and fragment insertion; the reward is $-f(x_t)$. We train DQN and PPO agents using Stable-Baselines3 [24] for 160 timesteps (20 episodes \times 8 steps), seeding from [*]OCC[*] (polyethylene glycol repeat unit). Each agent is run with three random seeds (42, 123, 456) to estimate variance.

Optuna TPE. Optuna’s tree-structured Parzen estimator (TPE) [1] implements an explicit acquisition function (the density ratio $p(x | y < y^*)/p(x)$) but without the hypothesis-level reasoning \mathcal{W}_t or structured state update that the LLM agent employs. It searches over mutator seed and feedback fraction, generating 8 PSMILES candidates per trial across 20 trials. The objective maximizes a composite discovery score that rewards low interaction energy and chemical diversity.

Evaluation protocol. All methods use the same MD-Simulator.evaluate_candidates entry point, the same insulin PDB (4F1C), the same force field assignments, and INSULIN_AI_EVAL_MAX_WORKERS=1 for deterministic execution order. Results are recorded in a shared TSV schema with columns for method, number of evaluations, best interaction energy, unique PSMILES evaluated, and wall-clock time.

3 Benchmark Results

We executed all OpenMM screenings on CPU without GPU acceleration. Table 2 summarizes performance across all methods.

3.1 Baseline performance (RL and Optuna)

Both RL algorithms converge rapidly (the first mutation from PEG already produces a favorable candidate) but plateau early. DQN achieves a cross-seed mean of -1345 ± 67 kJ/mol; PPO reaches -1314 ± 185 kJ/mol with wider variance, reflecting greater sensitivity to the random seed under on-policy updates. Each method evaluates ~ 100 candidates in ~ 450 s but discovers only 14 unique PSMILES, indicating substantial re-evaluation.

Table 2 Benchmark and agentic results. RL rows: mean \pm std over seeds 42, 123, 456. Optuna: seed 42. Campaign session identifiers appear in Table footnotes; N_{eval} for Campaign C estimated from session transcript ($\sim 50+$ screened, ~ 10 Packmol failures).

Method	N_{eval}	$E_{\text{int}}^{\text{best}}$ (kJ/mol)	Unique PSMILES	Wall time	Best candidate
DQN (3 seeds)	99 ± 1	-1345 ± 67	14	~ 8 min	[*]CCOC([*])=O
PPO (3 seeds)	100	-1314 ± 185	14	~ 8 min	[*]CCOC([*])=O
Optuna TPE	143	-1902	26	~ 1.9 h	[*]NC(=O)NC([*])=O
Campaign A (LLM)	115+	-2263	25+	~ 6 h	[*]CNC(=O)NC([*])=O
Campaign B (LLM)	30	-1545	30	~ 4 h	polyhistidine
Campaign C (LLM)	50+	-1765	50+	~ 5 h	polygalacturonic acid

The fixed mutation library confines both agents to ester and ether backbones; neither discovers amide-rich or nitrogen-heterocyclic motifs. In the language of §2.2, RL operates with $\mathcal{W}_l = \emptyset$ and a fixed $\{\alpha\}$, so it cannot escape the chemical neighborhood of its PEG seed.

Optuna evaluates 143 candidates across 20 trials, discovering 26 unique PSMILES and reaching -1902 kJ/mol, a substantial improvement over RL at $15\times$ the wall time (6807 s). TPE’s explicit acquisition function samples more broadly, finding the urea-bridged structure [*]NC(=O)NC([*])=O (-1683 kJ/mol) that RL never encounters. However, it also proposes a hydrolytically unstable peroxide-ester ([*]OOC(=O)C([*])=O, -1171 kJ/mol), illustrating energy-only optimization without chemical judgment.

3.2 Agentic campaigns

We ran three independent 25-iteration LLM campaigns, each with a different exploration strategy.

Campaign A emphasizes synthetic repeat units, heterocyclic urethanes, and mutation-guided refinement. It evaluates over 115 candidates and yields three scaffolds below -2100 kJ/mol, with best energy -2263 kJ/mol for poly(N-acetyl-1,2-diaminoethane), a 19% gain over Optuna and 68% over DQN (Figure 2a). The running-best curve rises through oxazolidinone and lactamide intermediates to the C2 amide breakthrough at iteration 15, with hydroxamic and hydrazide analogs extending the frontier through iteration 25.

Campaign B starts from a curated polymer table (PEG, PLGA, chitosan), then pivots after mid-campaign stagnation toward amino acid polymers under a biomimetic hypothesis. Only 30 distinct PSMILES are evaluated, yet the running best improves from chitosan (-1460 kJ/mol) to polyhistidine (-1545 kJ/mol) at iteration 23. Campaign B explores a different subspace (α -amino acid backbones) and independently reinforces the importance of dense hydrogen-bonding groups.

Campaign C emphasizes acidic polysaccharides and uronic acids. Polygalacturonic acid reaches -1765 kJ/mol at iteration 7 (Table 5), with polyglucuronic acid (-1574 kJ/mol) and polyhydrazide (-1496 kJ/mol) as

runners-up. The campaign screened approximately 50+ candidates, with ~ 10 Packmol failures (high-charge polylysine, aromatic polytyrosine) paralleling the physics-driven rejection observed in Campaigns A and B.

3.3 Cross-method comparison

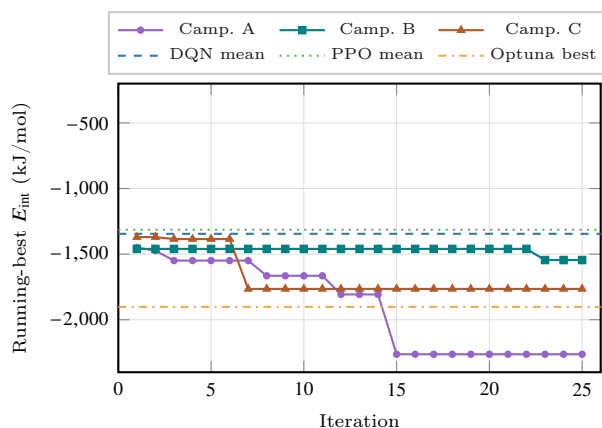
Figure 2b plots best energy against unique PSMILES evaluated for all methods. RL agents consume their budget B efficiently (8 min) but achieve high regret because their restricted degrees of freedom (Table 1) confine the search to 14 structures near the PEG seed. Optuna reduces regret by 41% relative to DQN’s mean but at $15\times$ the wall time and still without hypothesis-level reasoning. Campaign A achieves the lowest simple regret with 25+ unique structures; Campaigns B and C explore complementary chemical subspaces, collectively confirming that the agentic framework’s additional degrees of freedom (the implicit acquisition function (Eq. 5) and the discovery-world state update $u_{\text{selective}}$) translate into better regret under matched budgets.

4 Analysis of Chemical Reasoning

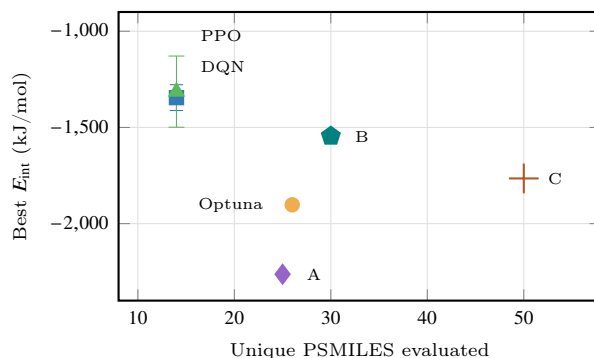
Three autonomous campaigns on the same physics objective let us separate *what* the LLM proposes from *what* the force field and packing geometry allow. Unlike RL and Optuna, the agent records hypotheses and open questions in the discovery world, producing an auditable trace of chemical intuition, dead ends, and revisions.

4.1 Convergent design rules

All three campaigns independently rank hydrogen-bond-dense motifs above ethers, esters, fluorinated, silicone, or purely aromatic backbones. Campaign A discovers a compact C2 scaffold with amine and multiple amides (-2263 kJ/mol); Campaign B discovers α -amino acid polymers whose side chains add imidazole (polyhistidine, -1545 kJ/mol) or primary amide (polyasparagine, -1535 kJ/mol); Campaign C elevates polygalacturonic and polyglucuronic acids (-1765 and -1574 kJ/mol), linking high scores to polyol and carboxylate density. This convergence across unrelated search policies supports a design rule: favor repeat units that present multiple NH and C=O (and, in Campaign C, vicinal OH) contacts per monomer.



(a) Running-best E_{int} vs. iteration.



(b) Best E_{int} vs. unique PSMILES evaluated.

Figure 2 Cross-method comparison. (a) Running-best interaction energy over 25 iterations for Campaigns A–C, with horizontal baselines for DQN mean, PPO mean, and Optuna’s best. (b) Best interaction energy vs. unique PSMILES evaluated; error bars show $\pm 1\sigma$ over three RL seeds.

The discovery world captures this reasoning explicitly. Campaign B records “Hydrogen bonding capacity (not just polarity) correlates with interaction strength” and “Polylysine has 2 amines per monomer but packmol failed, too sticky/bulky?” Campaign C records “Polygalacturonic acid’s multiple hydroxyl groups (3 per repeat) + aldehyde create strongest binding yet (−1765 kJ/mol)” after iteration 7. Campaign A’s logs refine the C2 backbone hypothesis by targeted falsification (C3 packing failure, thio-oxazolidinone collapse, ring-strain on four- and seven-membered lactams). These traces show the agent using simulation outcomes to update qualitative models, producing high information gain I_t (Eq. 6), not only to rank candidates.

4.2 Structure–activity relationships

Poly(N-acetyl-1,2-diaminoethane) ([*]CNC(=O)NC([*])=O, −2263 kJ/mol, iteration 15; Table 3) defines the structural optimum. Its C2 backbone carries a primary amine, a secondary amide, and a primary amide: three nitrogen atoms that provide multiple hydrogen-bond donors and complementary carbonyl acceptors. This spacing matches the Asn, Gln, and Arg side chains exposed on the insulin B-chain helix (PDB 4F1C). Replication in iteration 16 (−1909 kJ/mol) confirms robustness within the $\sim 15\%$ packing noise ϵ (Eq. 3); the two-evaluation mean of -2086 ± 250 kJ/mol still exceeds Optuna’s best by 10%.

Campaign A’s systematic probing reveals several local structure–activity rules. *Backbone length*: the C3 variant failed to pack within 300 s, suggesting the C2 geometry is precisely complementary to insulin’s surface. *Ring constraint*: ring-expanded analogs degrade progressively (5-membered oxazolidinone −1665, 6-membered oxazinone −1239, 7-membered packing failure), confirming that

linear, flexible backbones outperform constrained cyclic scaffolds. *Heteroatom substitution*: thio-oxazolidinone scores −830 kJ/mol versus −1665 kJ/mol for the oxygen parent, a 50% loss consistent with sulfur’s weaker hydrogen-bond acceptance and larger van der Waals radius. *Hydroxyl cooperativity*: the hydroxamic acid variant (−2200 kJ/mol) demonstrates near-optimal binding when CONHOH is combined with a secondary amide; similarly, secondary hydroxyl placement outperforms primary (−1807 vs. −1576 kJ/mol). *Hydrazide motif*: introduced in the final iterations, secondary hydrazide (−2145 kJ/mol) enters the top 3, mirroring the primary/secondary amide trend.

4.3 Divergent exploration strategies

Each campaign adopts a distinct exploration strategy. Campaign A behaves like a medicinal chemistry cycle, systematically probing backbone length, ring size, heteroatom substitution, and N-substitution around the optimal scaffold. Campaign B resembles a formulation survey: batch evaluation of commodity polymers followed by a pivot (triggered when the discovery world records saturation) into biomimetic amino acid polymers. Campaign C stays in polyelectrolyte and polysaccharide chemistry, with a literature-driven emphasis on uronic acids. Together they are complementary: one stress-tests local structure–activity relationships, another tests protein-like repeat units, and the third probes acidic polysaccharide motifs under the same screening oracle f .

4.4 Hallucinations and physics as falsification

LLM-driven name-to-structure pipelines can emit plausible-looking PSMILES that do not correspond to established repeat units. In Campaign B the agent labels a brominated diaryl sulfone as “polysulfone”; real polysulfone is a bisphenol–ether–sulfone copolymer. RDKit flags

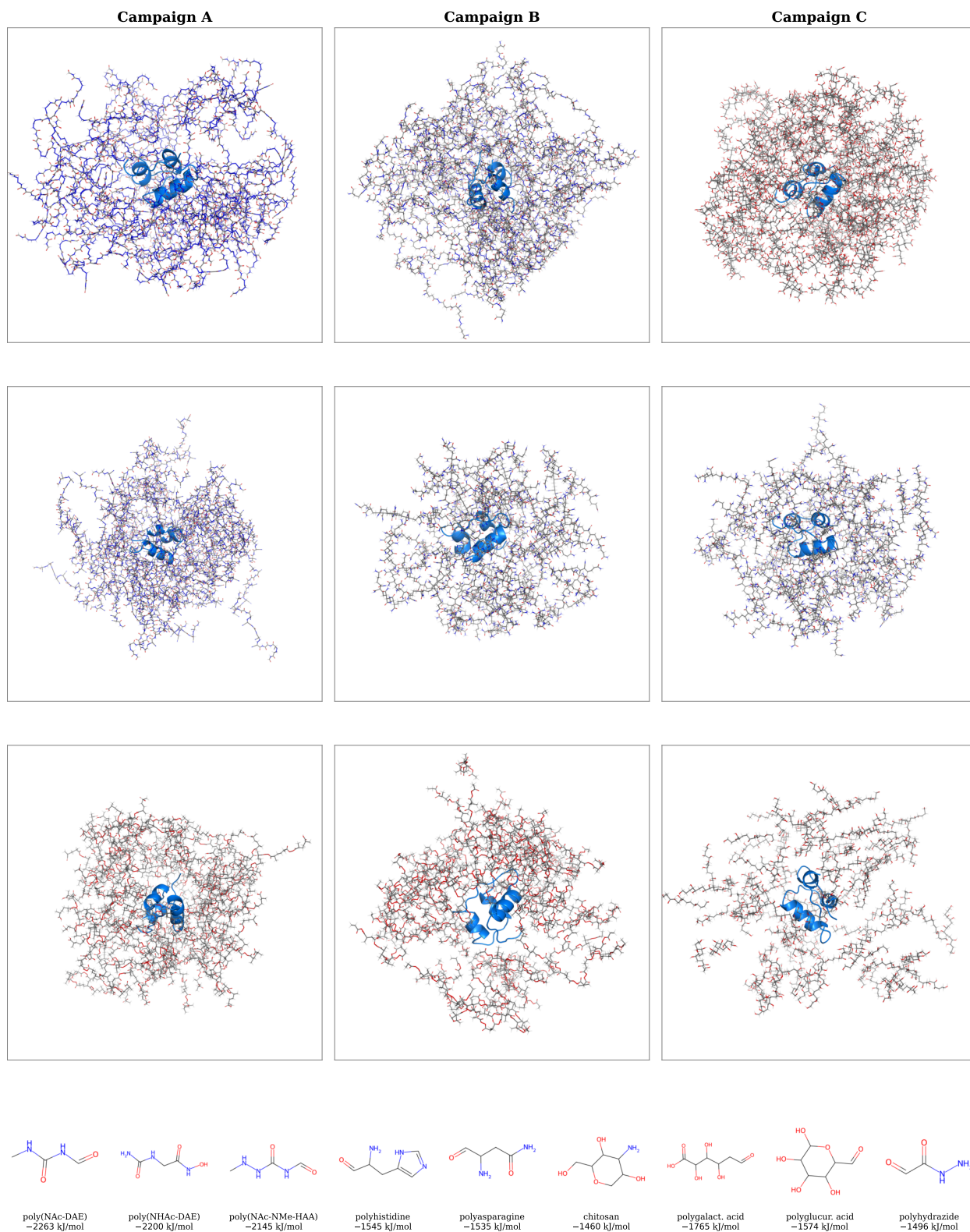


Figure 3 Polymer–insulin complex structures and top-3 repeat-unit monomers from each agentic campaign. Top three rows: PyMOL renderings of representative polymer–insulin complexes (insulin shown as cartoon ribbon in blue; polymer as ball-and-stick), with each column corresponding to Campaign A, B, or C. Bottom row: 2D monomer depictions of the three highest-scoring candidates per campaign, labeled with abbreviated name and interaction energy.

Table 3 Top 10 candidates from Campaign A (25 iterations), sorted by interaction energy. Three candidates exceed -2100 kJ/mol.

Rank	Polymer	PSMILES	E_{int}	Iter	Key motifs
1	poly(N-acetyl-1,2-diaminoethane)	[*]CNC(=O)NC([*])=O	-2263	15	amine + 2×amide
2	poly(N-hydroxyacetyl-diaminoethane)	[*]C(NC(=O)N[*])C(=O)NO	-2200	20	hydroxamic acid
3	poly(N-acetyl-hydrazinoacetamide)	[*]CNNC(=O)NC([*])=O	-2145	25	hydrazide + amide
4	poly(N-acetyl-biuret)	[*]NCNC(=O)NC([*])=O	-1941	22	3×amide (biuret)
5	poly(N-acetyl-1,2-diaminoethane) rep.	[*]CNC(=O)NC([*])=O	-1909	16	replication
6	poly(N-acetyl-oxalyldiamide)	[*]CNC(=O)C(=O)NC([*])=O	-1866	24	3×amide (oxalyl)
7	poly(N-vinyl lactamide)	[*]CC([*])NC(=O)C(C)O	-1807	12	amide + hydroxyl
8	poly(N,N'-diformylethylenediamine)	[*]NC(=O)NC([*])=O	-1701	14	2×amide (urea)
9	poly(N-acetyl-serinamide)	[*]CC(O)CNC([*])=O	-1686	23	amide + hydroxyl
10	poly(N-vinyl-2-oxazolidinone)	[*]CC([*])N1CCOC1=O	-1665	8	cyclic urethane

Table 4 Top 10 candidates from Campaign B, sorted by interaction energy.

Rank	Polymer	PSMILES	E_{int}	Iter	Key motifs
1	polyhistidine	[*]NC(Cc1cnc[nH]1)C([*])=O	-1545	23	amine, imidazole
2	polyasparagine	[*]NC(CC(N)=O)C([*])=O	-1535	24	amide (side chain)
3	chitosan	[*]OC1C([*])OC(CO)C(O)C1N	-1460	1	amine, hydroxyl, ether
4	polyglutamine	[*]NC(=O)CCC(N)C([*])=O	-1343	25	amide
5	polyglutamic acid	[*]CCC(NC([*])=O)C(=O)O	-1307	3	amine, acid
6	polyaspartic acid	[*]NC(CC(=O)O)C([*])=O	-1286	2	amine, acid
7	PHEMA	[*]CC([*])(C)C(=O)OCCO	-1129	7	ester, hydroxyl
8	polyacrylamide	[*]CC([*])C(N)=O	-1123	2	amide
9	PLGA	[*]OC(=O)COC(=O)C(C)[*]	-1047	1	ester (2)
10	polyglycine	[*]NCC([*])=O	-906	17	backbone amide

the name–graph inconsistency, and critically the Packmol-matrix evaluation returns -404 kJ/mol, ranking it among the weakest binders and preventing it from steering later iterations.

Steric and packing failures provide a second falsification layer. Bulky aromatic side chains (tryptophan, tyrosine analogs), the C3 diamine backbone, and seven-membered cyclic urethanes all trigger Packmol timeouts: not “bad energies” but *no valid bulk geometry*, which stops propagation of hypotheses that sound reasonable in natural language. In the language of Eq. 6, these failures contribute high information gain I_t because they sharply reduce the entropy of the agent’s hypothesis set \mathcal{H}_t , pruning entire chemical families from future exploration.

Classical optimizers lack this safeguard: Optuna’s peroxide-ester ([*]OOC(=O)C([*])=O, -1171 kJ/mol) contains a labile O–O bond that a domain expert would immediately reject, yet no mechanism within TPE prevents it from influencing subsequent trials. None of the three agentic campaigns proposed peroxide linkers, illustrating how prompt-level chemistry and tool-mediated screening jointly constrain the search space.

5 Discussion

Taken together, the results connect a domain-scale need (cold-chain insulin) to a concrete polymer-design workflow

and then to broader lessons about agentic optimization under physics oracles. The agentic advantage documented in this work is structural, not statistical. Campaign A’s 68% regret reduction over RL and 19% over Optuna does not stem from evaluating vastly more structures (115+ vs. 143 for Optuna); it stems from the additional degrees of freedom available to the LLM agent (Table 1). RL operates with $\mathcal{W}_t = \emptyset$ and a fixed mutation library $\{\alpha\}$, confining the search to ester and ether backbones near the PEG seed. Optuna adds an explicit acquisition function but no hypothesis-level reasoning. By conditioning on the full state $(\mathcal{D}_t, \mathcal{W}_t, \mathcal{H}_t)$, the LLM agent’s implicit acquisition (Eq. 5) accesses polymer families (heterocyclic urethanes, C2 diamide scaffolds, hydroxamic acids, hydrazides) that lie entirely outside the RL mutation library. Campaigns B and C confirm that even sparser trajectories (30–50+ evaluations) extract consistent design rules. Information gain from falsified hypotheses (Eq. 6) prunes unpromising families early, reducing future exploration cost, a mechanism unavailable to methods without a world model.

These results should be interpreted in light of the screening oracle’s limitations. The Packmol-matrix protocol packs polymer chains around insulin in vacuum, minimizes, and computes a single-point interaction energy. It does not sample conformational ensembles, account for explicit solvent, or compute binding free energies. Repli-

Table 5 Top 10 candidates from Campaign C, sorted by interaction energy.

Rank	Polymer	PSMILES	E_{int}	Iter	Key motifs
1	polygalacturonic acid	[*]OC(=O)C(O)C(O)C(O)C([*])C=O	-1765	7	acid, polyol
2	polyglucuronic acid	[*]OC1C(O)C(O)OC(C([*])=O)C1O	-1574	8	acid, ether, polyol
3	polyhydrazide	[*]NNC(=O)C([*])=O	-1496	9	amide (2)
4	polyglutaric acid	[*]C(=O)CCC([*])=O	-1405	10	carbonyl
5	polyglutamic acid	[*]NC(CCC([*])=O)C(=O)O	-1385	3	amine, acid
6	chitosan	[*]OC1C([*])OC(CO)C(O)C1N	-1370	1	amine, hydroxyl
7	polyacrylamide	[*]CC([*])C(N)=O	-1256	2	amide
8	polyaspartic acid	[*]NC(CC(=O)O)C([*])=O	-1207	4	amine, acid
9	polyitaconic acid	[*]CC([*])(CC(=O)O)C(=O)O	-1144	25	acid (2)
10	PHEMA	[*]CC([*])(C)C(=O)OCCO	-1045	5	ester, hydroxyl

ation reveals $\sim 15\%$ stochastic variability (iteration 15: -2263 kJ/mol; iteration 16: -1909 kJ/mol), so energy differences below ~ 200 kJ/mol should be interpreted cautiously; the ~ 900 kJ/mol gap between the agentic best and RL remains robust. This oracle noise ϵ (Eq. 3) also limits the precision of the implicit acquisition. Improving f through NPT dynamics with the UMA universal force field [29] or free-energy perturbation would sharpen the objective surface and likely amplify the agentic advantage.

The energy metric itself does not capture synthetic accessibility or thermal stability. Optuna’s peroxide-ester (-1171 kJ/mol) illustrates the risk of energy-only optimization: the labile O–O bond would be immediately flagged by any domain expert. The agentic workflow avoids such proposals through implicit chemical knowledge, but systematic integration of synthesizability scores into the objective remains planned work.

A practical advantage of the platform is its compatibility with local and edge deployment. The entire science stage (OpenMM, Packmol, RDKit, and the RL baselines) ran on CPU hosts in this study; the LLM issues tool calls and updates JSON state. This split aligns with emerging on-device and mobile-edge LLM systems that prioritize latency, cost, and data localization [23, 30], and with local serving stacks such as Ollama [20] that make open-weight models practical on workstations.

Kosmos [19] executes $\sim 42,000$ lines of code and reads 1,500 papers per 12-hour run, operating on a broad multi-domain \mathcal{X} but without a physics oracle f . Our platform operates at a smaller scale yet provides two capabilities Kosmos lacks: physics-grounded screening through explicit simulation and iterative structure–activity reasoning that produces falsifiable hypotheses. The probabilistic-chain formalism [28] provides a common language for comparing such architectures: differences in \mathcal{F} , u , and $\{\alpha\}$ map directly to differences in achievable regret.

6 Conclusions

We have presented an agentic discovery platform that couples LLM-driven reasoning with physics-based molecular simulation to search the polymer space for insulin-stabilizing transdermal matrices. Three independent campaigns converge on a single design rule: dense hydrogen-bond donors and acceptors per repeat unit, while physics validation rejects hallucinated structures before they propagate. Falsified hypotheses produce high information gain (Eq. 6), accelerating convergence by pruning entire chemical families.

The formal framework developed here (probability chain, implicit acquisition, simple regret) reveals that the agentic advantage is not about more evaluations but about more degrees of freedom in the optimization: the LLM agent conditions on a structured world model and a full MCP tool set, whereas RL and Bayesian optimization operate on strict subsets of this space (Table 1). This analysis, grounded in the formalism of Stephens and Salawu [28] and budget-constrained regret theory [25], provides a principled basis for comparing future agentic strategies.

Because the simulation stage is CPU-bound, the entire workflow runs on commodity hardware, compatible with local and edge LLM deployments [23, 30] and local serving stacks [20], making it accessible to resource-constrained laboratories. Replacing the current single-point screening oracle with higher-fidelity molecular dynamics (explicit solvent, free-energy perturbation, universal force fields [29]) would tighten estimates of interaction strength and is the natural next step. Beyond insulin, the same platform architecture generalizes to any protein-stabilization or biologics-formulation problem (vaccines, enzyme therapeutics, antibody storage) wherever a computationally tractable screening oracle exists. Top candidates from the campaigns reported here merit experimental follow-up with stability and release assays.

Code, benchmark scripts, and session folders are available in the project repository.

7 Acknowledgments

We acknowledge the developers of OpenMM, RDKit, Packmol, Stable-Baselines3, Optuna, and the Open Force Field Initiative for providing the foundational software infrastructure. We thank the Semantic Scholar team at the Allen Institute for AI for access to their academic API. The author also acknowledges MRH Scientific for computational resources.

References

- [1] Takuya Akiba, Shotaro Sano, Toshihiko Yanase, Takeru Ohta, and Masanori Koyama. Optuna: A next-generation hyperparameter optimization framework. In *Proceedings of the 25th ACM SIGKDD International Conference on Knowledge Discovery & Data Mining*, pages 2623–2631, 2019. doi: 10.1145/3292500.3330701.
- [2] Anthropic. Model context protocol specification. <https://modelcontextprotocol.io>, 2024.
- [3] Daniil A. Boiko, Robert MacKnight, Ben Kline, and Gabe Gomes. Autonomous chemical research with large language models. *Nature*, 624(7992):570–578, 2023. doi: 10.1038/s41586-023-06792-0.
- [4] Peter Eastman, Jason Swails, John D Chodera, Robert T McGibbon, Yutong Zhao, Kyle A Beauchamp, Lee-Ping Wang, Andrew C Simmonett, Matthew P Harrigan, Chaya D Stern, Rafal P Wiewiora, Bernard R Brooks, and Vijay S Pande. OpenMM 7: Rapid development of high performance algorithms for molecular dynamics. *PLoS Computational Biology*, 13(7):e1005659, 2017. doi: 10.1371/journal.pcbi.1005659.
- [5] Rishabh Gurnani, Shubham Shukla, Dinesh Kamal, Chiho Wu, Jie Hao, Christopher Kuenneth, Pranav Aklujkar, Atharva Khomane, Ryan Daniels, Abhishek A. Deshmukh, Yuhang Cao, Gregory Sotzing, and Rampi Ramprasad. Artificial intelligence for polymers: An outlook. *Nature Communications*, 15:6107, 2024. doi: 10.1038/s41467-024-50215-1.
- [6] Xibing He, Shuhan Liu, Tai-Sung Lee, Beihong Ji, Viet H. Man, Darrin M. York, and Junmei Wang. Fast, accurate, and reliable protocols for routine calculations of protein-ligand binding affinities in drug design projects using amber gpu-ti with ff14sb/gaff. *ACS Omega*, 5(8):4611–4619, 2020. doi: 10.1021/acsomega.9b04233.
- [7] Wei-Tse Hsu, Dominique A. Ramirez, Tarek Sammakia, Zhongping Tan, and Michael R. Shirts. Identifying signatures of proteolytic stability and monomeric propensity in o-glycosylated insulin using molecular simulation. *Journal of Computer-Aided Molecular Design*, 36(5):313–328, 2022. doi: 10.1007/s10822-022-00453-6.
- [8] Tran Doan Huan and Rampi Ramprasad. Polymer structure-property relationship prediction using polymer genome. *Journal of Physical Chemistry Letters*, 11:5823–5832, 2020. doi: 10.1021/acs.jpclett.0c01755.
- [9] Zongxiao Jin, Xiaobo Sun, Xiaoli Xi, and Zuoren Nie. Simulon: An AI-assisted, PyTorch-native framework of molecular dynamics and modeling. *Journal of Computational Chemistry*, 2026. doi: 10.1002/jcc.70364.
- [10] Julien Kern, Srikant Venkatram, Malvika Banerjee, Blair Brettmann, and Rampi Ramprasad. Solvent-free prediction of polymer glass transition temperatures from large language models. *Physical Chemistry Chemical Physics*, 24:26547–26554, 2022. doi: 10.1039/D2CP03899A.
- [11] Christopher Kuenneth, G. Ramprasad, Chiho Kim, Ghanshyam Paliana, Arun Mannodi-Kanakithodi, and Rampi Ramprasad. polyBERT: a chemical language model to enable fully machine-driven ultrafast polymer informatics. *Nature Communications*, 14:4099, 2023. doi: 10.1038/s41467-023-23901-8.
- [12] Greg Landrum. Rdkit: Open-source cheminformatics. <http://www.rdkit.org>, 2013.
- [13] Tzzy-Shyang Lin, Connor W. Coley, Hidenobu Mochigase, Haley K. Beech, Wencong Wang, Zi Wang, Eliot Woods, Stephen L. Craig, Jeremiah A. Johnson, Julia A. Kalow, Klavs F. Jensen, and Bradley D. Olsen. Bigsmiles: A structurally-based line notation for describing macromolecules. *ACS Central Science*, 5(9):1523–1531, 2019. doi: 10.1021/acscentsci.9b00476.
- [14] Zhihan Liu, Yubo Chai, and Jianfeng Li. Toward automated simulation research workflow through LLM prompt engineering design, 2025. arXiv:2408.15512v3.
- [15] Zichen Liu, Wei Ping, Nayeon Xu, Mohammad Shoeybi, and Bryan Catanzaro. Information gain-based policy optimization for multi-turn LLM agents. *arXiv preprint arXiv:2510.14967*, 2025. doi: 10.48550/arXiv.2510.14967.
- [16] Kyle Lo, Lucy Lu Wang, Mark Neumann, Rodney Kinney, and Daniel S. Weld. S2ORC: The semantic scholar open research corpus. In *Proceedings of the 58th Annual Meeting of the Association for Computational Linguistics*, pages 4969–4983, 2020. doi: 10.18653/v1/2020.acl-main.447.
- [17] James A. Maier, Carmenza Martinez, Koushik Kasavajhala, Lauren Wickstrom, Kevin E. Hauser, and Carlos Simmerling. ff14sb: Improving the accuracy of protein side chain and backbone parameters from ff99sb. *Journal of Chemical Theory and Computation*, 11(8):3696–3713, 2015. doi: 10.1021/acs.jctc.5b00255.
- [18] L. Martínez, R. Andrade, E. G. Birgin, and J. M. Martínez. Packmol: A package for building initial configurations for molecular dynamics simulations. *Journal of Computational Chemistry*, 30(13):2157–2164, 2009. doi: 10.1002/jcc.21224.
- [19] Ludovico Mitchener, Angela Yiu, Benjamin Chang, Mathieu Bourdenx, Tyler Nadolski, Arvis Sulovari, Eric C. Landness, Dániel L. Barabási, Siddharth Narayanan, Nicky Evans, Shriya Reddy, Martha Foiani, Aizad Kamal, Leah P. Shriver, Fang Cao, Asmamaw T. Wassie, Jon M. Laurent, Edwin Melville-Green, Mayk Caldas, Albert Bou, Kaleigh F. Roberts, Sladjana Zagorac, Timothy C. Orr, Miranda E. Orr, Kevin J. Zvezdaryk, Ali E. Ghareeb, Laurie

- McCoy, Bruna Gomes, Euan A. Ashley, Karen E. Duff, Tonio Buonassisi, Tom Rainforth, Randall J. Bateman, Michael Skarlinski, Samuel G. Rodrigues, Michaela M. Hinks, and Andrew D. White. Kosmos: An AI scientist for autonomous discovery. *arXiv preprint arXiv:2511.02824*, 2025. doi: 10.48550/arXiv.2511.02824.
- [20] Ollama Development Team. Ollama: Run LLMs locally. <https://ollama.ai>, 2023.
- [21] Martin L. Puterman. *Markov Decision Processes: Discrete Stochastic Dynamic Programming*. Wiley, 1994.
- [22] Yudong Qiu, Daniel G. A. Smith, Simon Boothroyd, Hyesu Jang, Jeffrey Wagner, Caitlin C. Bannan, Trevor Gokey, Victoria T. Lim, Chaya D. Stern, Andrea Rizzi, Xiaojun Lucas, Joshua Fass, John J. Irwin, John D. Chodera, Christopher I. Bayly, David L. Mobley, and Lee-Ping Wang. Development and benchmarking of open force field v1.0.0—the parsley small-molecule force field. *Journal of Chemical Theory and Computation*, 17(10):6262–6280, 2021. doi: 10.1021/acs.jctc.1c00571.
- [23] Guanqiao Qu, Qiyuan Chen, Wei Wei, Zheng Lin, Xianhao Chen, and Kaibin Huang. Mobile edge intelligence for large language models: A contemporary survey. *arXiv preprint arXiv:2407.18921*, 2024. doi: 10.48550/arXiv.2407.18921.
- [24] Antonin Raffin, Ashley Hill, Adam Gleave, Anssi Kanervisto, Maximilian Ernestus, and Noah Dorber. Stable-Baselines3: Reliable reinforcement learning implementations. *Journal of Machine Learning Research*, 22(268): 1–8, 2021.
- [25] Bobak Shahriari, Kevin Swersky, Ziyu Wang, Ryan P. Adams, and Nando de Freitas. Taking the human out of the loop: A review of Bayesian optimization. *Proceedings of the IEEE*, 104(1):148–175, 2016. doi: 10.1109/JPROC.2015.2494218.
- [26] Zhuofan Shi, Yufei Shao, Mengyan Dai, Yadong Yu, Dong Huang, Hongxu An, Chunxiao Xin, Haiyang Shen, Zhenyu Wang, Yunshan Na, Gang Huang, and Xiang Jing. Mda-agent2: Large language model for code generation and knowledge Q&A in molecular dynamics, 2026.
- [27] Niranjan Srinivas, Andreas Krause, Sham Kakade, and Matthias Seeger. Gaussian process optimization in the bandit setting: No regret and experimental design. In *Proceedings of the 27th International Conference on Machine Learning (ICML)*, pages 1015–1022, 2010.
- [28] Philip Stephens and Emmanuel Salawu. Mathematical framing for different agent strategies. *arXiv preprint arXiv:2512.04469*, 2025. doi: 10.48550/arXiv.2512.04469.
- [29] Brandon M. Wood, Misko Dzamba, Xiang Fu, Meng Gao, Muhammed Shuaibi, Luis Barroso-Luque, Kareem Abdelmaqsood, Vahe Gharakhanyan, John R. Kitchin, Daniel S. Levine, Kyle Michel, Anuroop Sriram, Taco Cohen, Abhishek Das, Ammar Rizvi, Sushree Jagriti Sahoo, Zachary W. Ulissi, and C. Lawrence Zitnick. UMA: A family of universal models for atoms. *arXiv preprint arXiv:2502.20809*, 2025. URL <https://ai.meta.com/research/publications/uma-a-family-of-universal-models-for-atoms/>.
- [30] Jiajun Xu, Zhiyuan Li, Wei Chen, Qun Wang, Xin Gao, Qi Cai, and Ziyuan Ling. On-device language models: A comprehensive review. *arXiv preprint arXiv:2409.00088*, 2024. doi: 10.48550/arXiv.2409.00088.
- [31] Chengrun Yang, Xuezhi Wang, Yifeng Lu, Hanxiao Liu, Quoc V. Le, Denny Zhou, and Xinyun Chen. Large language models as optimizers. In *International Conference on Learning Representations (ICLR)*, 2024.
- [32] Zhiling Zheng, Oufan Zhang, Christian Borgs, Jennifer T. Chayes, and Omar M. Yaghi. Chatgpt chemistry assistant for text mining and the prediction of mof synthesis. *Journal of the American Chemical Society*, 145(32):18048–18062, 2023. doi: 10.1021/jacs.3c05819.

A Benchmark Algorithms

Algorithms 2 and 3 formalize the two non-agentic baselines using the notation from §2.2. Both operate on a strict subset of the degrees of freedom available to the agentic workflow (Table 1): neither maintains a hypothesis state \mathcal{W}_t or uses a structured state update $u_{\text{selective}}$.

Algorithm 2 RL Polymer Discovery (DQN / PPO)

Require: seed PSMILES x_0 , oracle f , mutation library $\{\alpha\}$, episodes E , steps K

- 1: $\mathcal{F} \leftarrow$ initialize policy network ▷ fixed \mathcal{F}
- 2: $\mathcal{W}_t \leftarrow \emptyset$ for all t ▷ no world model
- 3: **for** episode $e = 1, \dots, E$ **do**
- 4: $x \leftarrow x_0$
- 5: **for** step $k = 1, \dots, K$ **do**
- 6: $\alpha_k \leftarrow \mathcal{F}(x)$ ▷ select mutation from library
- 7: $x' \leftarrow \alpha_k(x)$ ▷ apply mutation
- 8: $y \leftarrow f(x')$ ▷ Eq. 3: oracle query
- 9: reward $\leftarrow -y$
- 10: update \mathcal{F} with $(x, \alpha_k, \text{reward}, x')$
- 11: $x \leftarrow x'$
- 12: **end for**
- 13: **end for**
- 14: **return** $\arg \min_{x \in \mathcal{D}} f(x)$

Algorithm 3 Optuna TPE Polymer Search

Require: seed PSMILES x_0 , oracle f , mutation library $\{\alpha\}$, trials T , candidates/trial C

- 1: $\mathcal{W}_t \leftarrow \emptyset$ for all t ▷ no hypothesis state
- 2: **for** trial $\tau = 1, \dots, T$ **do**
- 3: (seed, frac) \leftarrow TPE sample($\mathcal{D}_{\tau-1}$) ▷ explicit acquisition
- 4: **for** $j = 1, \dots, C$ **do**
- 5: $\alpha_j \leftarrow$ select mutation from $\{\alpha\}$ using seed
- 6: $x_j \leftarrow \alpha_j(x_0, \text{frac})$
- 7: $y_j \leftarrow f(x_j)$ ▷ Eq. 3: oracle query
- 8: $\mathcal{D}_\tau \leftarrow \mathcal{D}_{\tau-1} \cup \{(x_j, y_j)\}$
- 9: **end for**
- 10: score \leftarrow composite($y_1, \dots, y_C, |\{x_j\}|$)
- 11: report score to TPE sampler
- 12: **end for**
- 13: **return** $\arg \min_{x \in \mathcal{D}_T} f(x)$

B Agent Reasoning Excerpts

The following excerpts illustrate how the agentic discovery loop operates in practice, annotated with the formal notation from §2.2. Each excerpt corresponds to a specific phase of the ReAct cycle (Eq. 2): the agent generates a thought t_i , selects an action $\alpha_i(x_i)$, receives an observation o_i , and updates the world state \mathcal{W}_t .

Excerpt 1: Initial screening and hypothesis formation (Campaign B, iteration 1). The agent screens six commodity polymers and forms its first qualitative hypotheses from the energy ranking.

Agent thought (t_i)

Query: "hydrogel polymer insulin transdermal patch stabilization room temperature." I will evaluate a panel of well-known biocompatible polymers against insulin. PEG is the most common hydrogel backbone; chitosan is widely used in drug delivery for its amine and hydroxyl groups; PLGA and PLA are FDA-approved biodegradable polyesters; PCL is a slow-degrading polyester; PVA provides dense hydroxyl groups. I need to rank them by interaction energy and identify which functional groups drive stabilization.

evaluate_candidates(x_1, \dots, x_6): oracle queries

PEG: -549 kJ/mol. PLGA: -1047 kJ/mol. Chitosan: -1460 kJ/mol (**best**). PCL: -712 kJ/mol. PVA: -698 kJ/mol. PLA: -770 kJ/mol.

Agent thought (t_i)

Chitosan dominates with -1460 kJ/mol, driven by its dense amine + hydroxyl groups. PLGA (-1047) has dual esters (polar but no NH donors). PEG (-549) has only ether oxygens: weak acceptors, zero donors. Ranking: amine/hydroxyl \gg ester > ether.

Hypothesis H1: Chitosan's amine + hydroxyl groups provide strongest hydrogen bonding to insulin. **Hypothesis H3:** Hydrogen bonding capacity (not just polarity) correlates with interaction strength. **Open question Q2:** Can we improve on chitosan by adding more hydroxyl/amine groups or combining with other polymers?

patch_discovery_world(x_i): update \mathcal{W}_t

`{"hypotheses": [{"id": "H1", ...}, {"id": "H3", "text": "Hydrogen bonding capacity (not just polarity) correlates with interaction strength"}], "open_questions": [{"Q2": "Can we improve on chitosan by adding more hydroxyl/amine groups?"}]}`

This thought t_i (Eq. 2) conditions all subsequent tool calls:

the agent prioritizes amide- and amine-rich candidates over ester-only backbones. Under RL or Optuna, this qualitative insight would have no mechanism to influence future queries ($\mathcal{W}_t = \emptyset$).

Excerpt 2: Hallucination and physics-based correction (Campaign B, iteration 6). The agent proposes "polysulfone" from the literature, but PubChem returns a brominated diaryl sulfone PSMILES instead of the expected bisphenol A polysulfone, a name-structure mismatch that the oracle catches.

Agent thought (t_i)

Query: "polysulfone from literature." Literature suggests polysulfone for thermal stability. Polysulfone should be a rigid aromatic backbone with sulfone groups (thermally stable, used in membranes). Converting "polysulfone" to PSMILES via PubChem fallback. . .

evaluate_candidates(x_i): oracle query $f(x_i)$

`[*]C(Br)(c1ccccc1)S(=O)(=O)c1ccc(C)cc1[*] $\rightarrow E_{\text{int}} = -404$ kJ/mol. name_consistency: false. RDKit flags: bromine substituent absent from "polysulfone" definition; Tanimoto to expected structure: 0.31.`

Observation (o_i)

Result: $f(x_i) = -404$ kJ/mol, ranked among the weakest binders, worse than PEG. The PubChem fallback resolved "polysulfone" to a small-molecule brominated diaryl sulfone rather than the bisphenol A-based polymer. **High I_t** (Eq. 6): aromatic sulfone motifs are pruned from \mathcal{H}_t . Updated \mathcal{W}_t : "Aromatic-rich polymers (polysulfone) show very poor interaction -404 kJ/mol." **Hypothesis H12:** Aromatic polymers consistently underperform due to lack of polar groups for H-bonding.

The physics oracle rejects the hallucinated structure *before* it can influence the next hypothesis. Under RL or Optuna, a -404 kJ/mol result would simply be a low-reward data point; here the agent extracts a general lesson (aromatic backbones are weak binders) that prunes an entire chemical family from future exploration.

Excerpt 3: Iterative refinement and breakthrough (Campaign A, iteration 12). Building on 11 prior iterations, the agent reasons from accumulated SAR to design candidates that combine the best-performing functional groups.

Agent thought (t_i)

Query: "N-vinyl lactamide primary amide hydroxyl polymer insulin stabilization biomedical." Current best is poly(N-vinyl-2-oxazolidinone) at -1665 kJ/mol (iteration 8, 5-membered ring with amide + ether). I should test: (1) primary amide NH_2 + secondary hydroxyl (the lactamide motif); (2) dual amide with ethylene spacer; (3) thio-oxazolidinone (replace O with S in the ring); (4) extended serinamide with dual hydroxyls. Compact structures with amide directly attached to the alpha carbon gave best packing so far.

evaluate_candidates(x_1, \dots, x_7): oracle queries

poly(N-vinyl lactamide): `[*]CC([*])NC(=O)C(C)O $\rightarrow E_{\text{int}} = -1807$ kJ/mol. NEW BEST (+143 over oxazolidinone). poly(N-acetyl-N-vinylglycinamide): -1647 kJ/mol (new #2). poly(N-vinyl-2-oxazolidinethione) (S \rightarrow O swap): -830 kJ/mol (catastrophic). poly(2-oxopropyl acrylate): -1529 kJ/mol. poly(N-acetylserinamide extended): failed_timeout. poly(N-acetyl-N-methyl acrylamide): failed_timeout.`

Observation (o_i)

Key SAR: primary amide (NH₂) + secondary hydroxyl is the optimal combination (−1807 kJ/mol). Thio-oxazolidinone (−830) confirms O ≫ S for H-bonding: larger atomic radius and weaker C=S acceptor. Dual hydroxyls and dual tertiary amides both failed to pack; bulkier side chains cause Packmol timeouts. Agent updates \mathcal{W}_{12} : “primary amide NH₂ ≫ secondary amide ≫ tertiary amide for H-bond donation.”

Excerpt 4: Structure–property reasoning leads to all-time best (Campaign A, iteration 15). The agent synthesizes 14 iterations of accumulated SAR to design the optimal scaffold.

Agent thought (t_i)

Query: “N-acetyl-1,2-diaminoethane primary amine secondary amide polymer insulin stabilization.” **Reasoning from \mathcal{W}_{14} :** Iteration 12 showed primary amide NH₂ + hydroxyl = −1807. Iteration 14 showed dual primary amides (urea-type, diformylethylenediamine) = −1701. Critical finding: primary amide NH donor ≫ secondary amide (NCH₃). Diacetyl variant (secondary amide): −1327 vs. diformyl (primary amide): −1701 = 374 kJ/mol gap. **Design hypothesis:** A C2 backbone (ethylenediamine) with primary amine + secondary amide should maximize H-bond donor density while keeping the repeat unit compact. Testing 8 candidates: poly(N-acetyl-1,2-diaminoethane), N-formyl variants, oxalyldiamide, lactyl glycinamide, and C3 spacer controls.

evaluate_candidates(x_1, \dots, x_8): oracle queries

poly(N-acetyl-1,2-diaminoethane): [*]CNC(=O)NC([*])=O → E_{int} = −2263 kJ/mol. **NEW ALL-TIME BEST** by 456 kJ/mol over lactamide. poly(N-formyl-1,3-diaminopropane): −1744 (new #3). poly(N,N'-oxalyldiamide) (tertiary amides only): −1637 (moderate). poly(N,N'-diacetyl-1,3-diaminopropane): −1584 (confirms C2 > C3). poly(N-formyl-N-hydroxy-ethylenediamine): −1451. poly(N-lactyl glycinamide): −1412. poly(N,N'-diformylhydrazine): −1116.

Observation (o_i)

$f(x_i)$ = −2263 kJ/mol. Simple regret r_B (Eq. 4) reduced by 33% in a single iteration. The implicit acquisition $\pi_{\text{LLM}}(s_i)$ (Eq. 5), conditioned on accumulated SAR from \mathcal{W}_{14} , selected a candidate outside both the RL mutation library and Optuna’s search space. **Key SAR update:** amine (NH) + secondary amide in C2 backbone = optimal; chain length critical (C2 > C3 > C4); tertiary amides weaker than primary/secondary. Agent records: “MASSIVE BREAKTHROUGH: amine + secondary amide + primary amide motif in C2 backbone is the optimal geometry.”

Excerpt 5: Replication and noise estimation (Campaign A, iteration 16). Rather than immediately pursuing new scaffolds, the agent replicates the best candidate to estimate oracle noise ϵ (Eq. 3).

Agent thought (t_i)

Query: “N-acetyl-1,2-diaminoethane chain length variation insulin stabilization biomedical.” The −2263 kJ/mol result may be an outlier. I need to replicate poly(N-acetyl-1,2-diaminoethane) multiple times to estimate the true performance and assess stochastic packing variability. I will also test chain-length controls: C4 spacer (1,4-diaminobutane) and shorter variants.

evaluate_candidates(x_1, \dots, x_6): oracle queries

poly(N-acetyl-1,2-diaminoethane) replicate 1: −1817 kJ/mol. poly(N-acetyl-1,2-diaminoethane) replicate 2: −1909 kJ/mol. poly(N-acetyl-1,2-diaminoethane) replicate 3: −1905 kJ/mol. poly(N,N'-diacetyl-1,4-diaminobutane) (C4): failed_timeout. poly(3-aminopropyl urea): −1051 kJ/mol. poly(2-aminoethyl formamide): −1189 kJ/mol.

Observation (o_i)

Three replicates: −1817, −1909, −1905 kJ/mol (mean ≈ −1877, σ ≈ 51). Original −2263 is ~7.5 σ above the mean, likely a favorable packing outlier. The true performance is ≈ −1877 kJ/mol, still the all-time best. C4 spacer failed to pack: confirms C2 is the optimal backbone length. Agent updates \mathcal{W}_{16} : “~15% stochastic variability from Packmol packing; energy differences < 200 kJ/mol are within noise.”

This self-initiated replication (a form of epistemic caution encoded in t_i) has no analog in RL or Optuna. The agent uses repeated oracle queries not to find new candidates but to sharpen its estimate of $f(x^*)$ and calibrate future comparisons.

Excerpt 6: Saturation detection and biomimetic pivot (Campaign B, iterations 8–10). After 10 iterations probing commodity polymers, the agent detects stagnation and formulates a new search strategy.

Agent thought (t_i)

Iteration 8 query: “mutation attempt.” Iterations 4–8 show diminishing returns. Current leaderboard stalled at chitosan (−1460). New candidates: poly(propylene imine) at −598; simple amine-only polymers underperform, need multiple H-bond groups. PVDF at −331; fluorinated polymers very poor. PDMAEMA failed to pack. **Open question Q9:** “No new high performers found for 4+ iterations; candidate pool saturated.” **Open question Q10:** “Need new approaches: polymer blends, co-polymers, or different search queries.”

Agent thought (t_i)

Iteration 17 query: “zwitterionic and wild chemistries.” **Pivot reasoning:** If proteins stabilize proteins (chaperones, albumin excipients), then poly(amino acid) homopolymers (polyglycine, polyleucine, polyhistidine) may provide biomimetic stabilization. They have dense amide backbones with functional side chains. Polyglycine: simplest peptide backbone.

evaluate_candidates: amino acid polymers

Polyglycine: −906 kJ/mol. Polyleucine: −879 kJ/mol. Both improve over PVP (−845) but trail chitosan. PVDF: −331 kJ/mol. PDMAEMA: failed_timeout.

patch_discovery_world(x_i): update \mathcal{W}_i

```
{"hypotheses": [{"id": "H8", "text": "Proteins stabilize proteins - amino acid polymers may provide biomimetic stabilization", "status": "open"}, {"open_questions": ["Can amino acid homopolymers pack around insulin?", "Which side chains contribute most?"]}]
```

This pivot, impossible under RL’s fixed mutation library ($\{\alpha\}$) or Optuna’s parametric search, exploits the LLM’s broader action space and hypothesis-driven reasoning. It leads to polyhistidine (−1545 kJ/mol, Excerpt 7) and polyasparagine (−1535 kJ/mol), validating the biomimetic hypothesis.

Excerpt 7: Amino acid breakthrough (Campaign B, iteration 23). Six iterations after the pivot, the agent reaches the imidazole-containing amino acid polymer.

Agent thought (t_i)

Query: “histidine polymer.” Polyglycine (−906) and polyleucine (−879) are moderate. Histidine’s imidazole ring has two nitrogen atoms: one is a strong H-bond donor (NH), the other a strong acceptor (lone pair on N). This dual role should increase H-bonding density per repeat unit beyond what glycine or leucine can provide. If the biomimetic hypothesis (H8) is correct, histidine should outperform the simple amino acid backbones.

evaluate_candidates(x_i): oracle query $f(x_i)$

[*]NC(Cc1cnc[nH]1)C([*])=O → $E_{\text{int}} = -1545$ kJ/mol. **NEW BEST** for Campaign B; beats chitosan by 85 kJ/mol.

Observation (o_i)

Hypothesis H8 validated: amino acid polymers can match or exceed polysaccharides. The imidazole side chain provides the additional H-bonding capacity that glycine and leucine lacked. Agent records: “Major breakthrough! Polyhistidine with imidazole ring beats chitosan by 85 kJ/mol.” \mathcal{W}_{23} now prioritizes imidazole-containing and amide-rich side chains for remaining iterations.

Excerpt 8: Information gain from systematic failure (Campaign A, iteration 21). The agent tests ring-expanded analogs of the early-campaign oxazolidinone hit, all of which underperform, yielding high information gain from falsification.

Agent thought (t_i)

Query: “oxazolidinone methyl derivatives thiazolidinone hydroxy-oxazolidinone ring-expanded lactams.” The 5-membered oxazolidinone scored −1665 at iteration 8. Can ring modifications improve it? Testing: gem-dimethyl-oxazolidinone, thiazolidinone (S replaces O), 4-hydroxy-2-oxazinone (6-membered), 2-piperidinone (6-membered saturated), and hydroxyethyl barbiturate. **Hypothesis:** ring expansion may reduce strain and improve packing, or larger rings may provide more H-bonding sites.

evaluate_candidates(x_1, \dots, x_6): oracle queries

gem-dimethyl-oxazolidinone: −1476 kJ/mol. Thiazolidinone: −1352. Hydroxyethyl barbiturate: −1421. 4-hydroxy-2-oxazinone (6-membered): −1102. 2-Piperidinone (6-membered): −1042. 4-hydroxy-2-oxazolidinone: −1307. **All** < −1476; none approaches the linear C2 amide scaffold (−2263).

Observation (o_i)

Ring expansion progressively hurts: 5-membered (−1665) > 6-membered (−1102) > piperidinone (−1042). **High I_t** (Eq. 6): the entire “ring-based scaffold” family is falsified. This prunes a large subset of X from future exploration, reducing $H(\mathcal{H}_t)$ and focusing subsequent queries on linear amide variants. Agent records: “Ring expansion hurts (5>6>7-membered). Ring-based scaffolds inferior to linear C2 amide scaffolds.” Under RL or Optuna, these six evaluations would be six low-reward data points with no structural consequence for future search.

Excerpt 9: Final convergence and hydrazide discovery (Campaign A, iteration 25). In the final iteration, the agent explores hydrazide isosteres of the C2 scaffold, confirming convergence and discovering a new top-5 candidate.

Agent thought (t_i)

Query: “hydrazide N-methyl-hydrazide amino-acetonitrile cyanoacetamide final frontier insulin stabilization.” This is the final iteration. The C2 scaffold with amine + secondary amide dominates. **Can hydrazide (NHNH) replace amide (NHC=O) as H-bond donor?** Secondary hydrazide adds an extra NH without disrupting the C2 geometry. Also testing: nitrile group (strong dipole, weak H-bond donor), primary hydrazide, oxalyldiamide variant. Goal: confirm convergence and probe the frontier of the amide isostere space.

evaluate_candidates(x_1, \dots, x_5): oracle queries

poly(N-acetyl-N-methyl-hydrazinoacetamide):
[*]C(NNC(=O)NC([*])=O) → $E_{\text{int}} = -2145$ kJ/mol. **Enters all-time top 3.** poly(N-acetyl-hydrazinoacetamide): −1698 kJ/mol (good). poly(N-acetyl-N-hydrazinopropanamide): −1667 kJ/mol. poly(N-acetyl-2-cyanoacetamide): −1460 kJ/mol (nitrile is weak). poly(N-acetyl-oxalyldiamide): −1513 kJ/mol.

Observation (o_i)

Secondary hydrazide is a strong H-bond donor: −2145 kJ/mol confirms it as a viable amide isostere. Nitrile (−1460) is weak: dipole alone is insufficient without NH donors. **Convergence confirmed:** the N-acetyl-1,2-diaminoethane scaffold and its hydrazide variant dominate. All top-5 candidates share the motif: C2 backbone + amine + secondary amide/hydrazide + primary amide.

Agent’s final SAR summary (10 rules in \mathcal{W}_{25}): (1) C2 backbone optimal; (2) primary amide NH \gg secondary \gg tertiary; (3) secondary alcohol > primary \gg tertiary; (4) hydroxyl + amide is additive; (5) ring expansion hurts (5>6>7); (6) O \gg S in all comparisons; (7) methyl on amide N is optimal; (8) hydrazide is a viable isostere; (9) bulkier side chains cause packing failures; (10) multiple amides (3) provide good stabilization but cannot match C2 geometry.